

# MOLECULAR EMISSION FROM A GALAXY ASSOCIATED WITH A $Z \sim 2.2$ DAMPED LYMAN-ALPHA ABSORBER

MARCEL NEELEMAN<sup>1,2</sup>, NISSIM KANEKAR<sup>3</sup>, J. XAVIER PROCHASKA<sup>1</sup>, LISE CHRISTENSEN<sup>4</sup>, MIROSLAVA DESSAUGES-ZAVADSKY<sup>5</sup>, JOHAN P.U. FYNBO<sup>6</sup>, PALLE MØLLER<sup>7</sup>, MARTIN A. ZWAAN<sup>7</sup>

*Draft version March 19, 2018*

## ABSTRACT

Using the Atacama Large Millimeter/sub-millimeter Array, we have detected CO(3–2) line and far-infrared continuum emission from a galaxy associated with a high-metallicity ( $[M/H] = -0.27$ ) damped Ly- $\alpha$  absorber (DLA) at  $z_{\text{DLA}} = 2.19289$ . The galaxy is located  $3.5''$  away from the quasar sightline, corresponding to a large impact parameter of 30 kpc at the DLA redshift. We use archival Very Large Telescope-SINFONI data to detect H $\alpha$  emission from the associated galaxy, and find that the object is dusty, with a dust-corrected star formation rate of  $110_{-30}^{+60} M_{\odot} \text{ yr}^{-1}$ . The galaxy’s molecular mass is large,  $M_{\text{mol}} = (1.4 \pm 0.2) \times 10^{11} \times (\alpha_{\text{CO}}/4.3) \times (0.57/r_{31}) M_{\odot}$ , supporting the hypothesis that high-metallicity DLAs arise predominantly near massive galaxies. The excellent agreement in redshift between the CO(3–2) line emission and low-ion metal absorption ( $\sim 40 \text{ km s}^{-1}$ ) disfavors scenarios whereby the gas probed by the DLA shows bulk motion around the galaxy. We use Giant Metrewave Radio Telescope HI 21 cm absorption spectroscopy to find that the HI along the DLA sightline must be warm, with a stringent lower limit on the spin temperature of  $T_s > 1895 \times (f/0.93) \text{ K}$ . The detection of CI absorption in the DLA, however, also indicates the presence of cold neutral gas. To reconcile these results requires that the cold components in the DLA contribute little to the HI column density, yet contain roughly 50% of the metals of the absorber, underlining the complex multi-phase nature of the gas surrounding high- $z$  galaxies.

*Subject headings:* quasars: absorption lines — galaxies: high-redshift — galaxies: ISM — submillimeter: galaxies — galaxies: kinematics and dynamics

## 1. INTRODUCTION

Absorption spectroscopy of quasars, to this day, remains the most efficient way to study HI at high redshifts. The strongest HI absorbers, the so-called damped Ly- $\alpha$  absorbers (DLAs; e.g., Wolfe et al. 2005) have HI column densities  $\geq 2 \times 10^{20} \text{ cm}^{-2}$  and contain the vast majority ( $> 80\%$ ) of HI at high redshifts (e.g., Péroux et al. 2003). DLAs are expected to be closely associated with galaxies because of the well-established correlation between HI and star formation (e.g. Schmidt 1959), and because in the local universe HI column densities comparable to DLAs occur primarily in galaxy disks. However, the nature of the galaxies associated with DLAs remains an open question, with simulations (e.g., Bird et al. 2014) predicting dark matter halo masses significantly smaller than those inferred from DLA cross-correlation observa-

tions (Pérez-Ràfols et al. 2018).

Over the last three decades, many attempts have been made to image the galaxies associated with DLAs directly in emission (e.g., Le Brun et al. 1997; Møller et al. 2002; Chen et al. 2005). These studies have been moderately successful at low redshift, but despite valiant efforts using innovative observation techniques (e.g. Kulkarni et al. 2006; Fynbo et al. 2010; Fumagalli et al. 2015; Johnson-Groh et al. 2016), fewer than 20 absorber-galaxy pairs are known at  $z \gtrsim 2$  (Krogager et al. 2017). With the commissioning of efficient integral field unit (IFU) spectrographs on 10 m-class telescopes, the ability to detect galaxy-absorber pairs has significantly improved (e.g., Péroux et al. 2011; Bouché et al. 2013; Jorgenson & Wolfe 2014; Fumagalli et al. 2017). However, all of these studies aim at detecting the emission from the stars and the ionized regions of galaxies, which may be highly obscured in a dusty galaxy. The Atacama Large Millimeter/sub-millimeter Array (ALMA) provides a complementary approach, whereby we can search for longer wavelength emission (e.g., from CO, [CII] lines, and radio continuum), which is less affected by the presence of dust and arises predominantly from the molecular and atomic gas inside the galaxy.

In Neeleman et al. (2016), we presented the first detection of molecular emission from a galaxy associated with a Ly- $\alpha$  absorber. In subsequent work, we found that molecular emission is detected in a large fraction of galaxies associated with high-metallicity absorbers at  $z \approx 0.7$ , and that their gas fraction is significantly higher than that of emission-selected galaxies at these redshifts (Møller et al. 2018; Kanekar et al. 2018). Encouraged by

Email: neeleman@mpia-hd.mpg.de

<sup>1</sup> Department of Astronomy & Astrophysics, UCO/Lick Observatory, University of California, 1156 High Street, Santa Cruz, CA 95064, USA

<sup>2</sup> Max-Planck-Institut für Astronomie, Königstuhl 17, D-69117, Heidelberg, Germany

<sup>3</sup> Swarnajayanti Fellow; National Centre for Radio Astrophysics, Tata Institute of Fundamental Research, Pune 411007, India

<sup>4</sup> Dark Cosmology Centre, Niels Bohr Institute, Copenhagen University, Juliane Maries Vej 30, DK-2100 Copenhagen O, Denmark

<sup>5</sup> Observatoire de Genève, Université de Genève, 51 Ch. des Maillettes, 1290 Versoix, Switzerland

<sup>6</sup> Cosmic Dawn Center, Niels Bohr Institute, Copenhagen University, Juliane Maries Vej 30, DK-2100 Copenhagen O, Denmark

<sup>7</sup> European Southern Observatory, Karl-Schwarzschildstraße 2, D-85748 Garching bei München, Germany

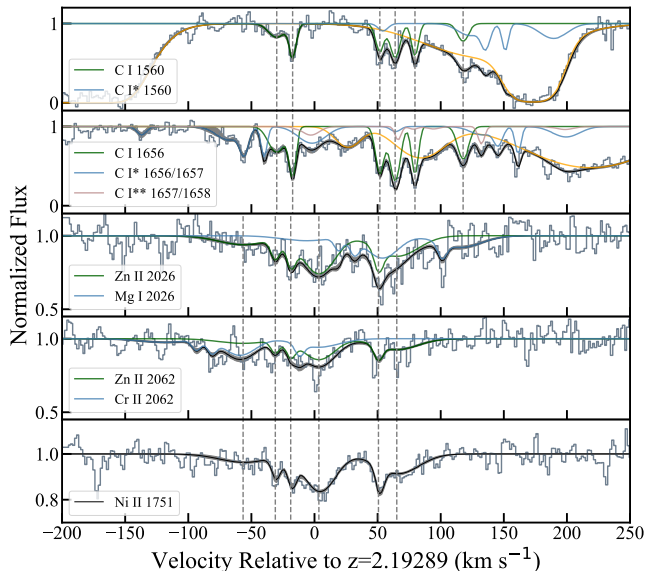


FIG. 1.— Selection of absorption lines in the VLT-UVES spectrum. The median model (black line) and  $1\sigma$  uncertainties (gray region) from the MCMC fitting routine as well as individual metal lines are shown. The vertical (gray) dashed lines mark the six velocity components of the C I, Zn II, and Ni II metal lines. The yellow lines in the top two panels are absorption features due to higher redshift intervening H I systems. The velocity offsets for Mg I and Cr II are  $50 \text{ km s}^{-1}$  and  $-63 \text{ km s}^{-1}$ , respectively. Note the lack of C I absorption in the strongest Zn II and Ni II component at  $v \approx 3 \text{ km s}^{-1}$ .

these results, we have targeted three DLAs at  $z \sim 2$  with ALMA to search for CO emission from galaxies associated with the absorbers. One of them—the DLA toward QSO B1228–113 (Ellison et al. 2001)—is the focus of this Letter; the remaining two systems will be discussed in a future paper. Throughout this Letter we assume a standard flat Lambda Cold Dark Matter cosmology with  $\Omega_{\Lambda} = 0.7$ , and  $H_0 = 70 \text{ km s}^{-1}$ .

## 2. OBSERVATIONS

### 2.1. UVES Observations

To search for metal lines from the DLA, a high resolution spectrum was obtained of QSO B1228–113 using the Ultraviolet and Visual Echelle Spectrograph (UVES; Dekker et al. 2000) on the Very Large Telescope (VLT). Details of the observations and reduction procedures are described in Akerman et al. (2005). By fitting a single component to the Zn II absorption line, these authors reported a metallicity of  $[M/H] = -0.22$ . To provide an updated measure of the metallicity, we have renormalized the spectrum, and refitted the metal lines using a Monte Carlo Markov Chain Voigt profile fitting routine publicly available in the LINETOOLS<sup>8</sup> package (Prochaska et al. 2017).

Specifically, we fit the Ni II  $\lambda 1741$  and Ni II  $\lambda 1751$  lines with six absorption components to provide an accurate model of the absorption profile. We then tie the component structure of the blended lines (i.e., Zn II, Mg I, and Cr II) to the Ni II lines assuming turbulent broadening (see e.g., Prochaska & Wolfe 1997) leaving only the total column density as a variable. This yields a Zn II column

density of  $\log(N(\text{Zn II})/\text{cm}^{-2}) = 12.96 \pm 0.03$ , resulting in an updated metallicity of  $[M/H] = -0.27 \pm 0.10$ , consistent with the previous measurement. The VLT-UVES spectrum also showed absorption from the ground and excited fine structure states of neutral carbon (C I, C I\* and C I\*\*). A 6-component fit of this complex is shown in Figure 1. The redshift, relative strength and Doppler parameters of the C I lines are different from the other low-ionization lines, as this line traces the coldest components of the gas (e.g., Jorgenson et al. 2010). The total column densities of the different species are listed in Table 1.

### 2.2. ALMA Observations

The field surrounding QSO B1228–113 was observed with ALMA on UT 2017 April 7 and 8 with a compact configuration (maximum baseline of 453 m) for a total on-source integration time of 2.4 hours. One of the four spectral windows was centered on the redshifted CO(3–2) line at 108.3 GHz, and the remaining three spectral windows were set up to measure continuum emission. Callisto and Ganymede were used as flux calibrators, while QSO J1256–0547 and QSO J1216–1033 were used for bandpass and phase calibration, respectively.

The initial calibration was carried out using the ALMA pipeline in the Common Astronomy Software Applications (CASA; McMullin et al. 2007) package. The quasar continuum flux density ( $18.8 \text{ mJy}$ ; left panel Figure 2) was sufficient to perform self-calibration, which was done in the Astronomical Image Processing System (AIPS; Greisen 2003) package. The continuum image was created in CASA using natural weighting, resulting in a synthesized beam of  $2.9'' \times 2.0''$  at  $-83.8^\circ$  and a root mean square (RMS) noise of  $6.9 \mu\text{Jy beam}^{-1}$ . The spectral cube was Hanning-smoothed to a velocity resolution of  $43.2 \text{ km s}^{-1}$ . The resulting, naturally weighted spectral cube has a mean synthesized beam of  $2.6'' \times 1.8''$  at  $-83.4^\circ$ , and an RMS of  $0.15 \text{ mJy beam}^{-1}$  per  $43.2 \text{ km s}^{-1}$  channel.

A clear emission line is detected in the continuum-subtracted spectral cube with a full width at half maximum (FWHM) of  $600 \pm 60 \text{ km s}^{-1}$  and a velocity-integrated flux density of  $0.73 \pm 0.06 \text{ Jy km s}^{-1}$  (Table 2

TABLE 1  
PROPERTIES OF THE ABSORBER  
DLA B1228–113

Right Ascension (J2000)	12:30:55.62
Declination (J2000)	-11:39:09.9
Redshift	2.19289
$\log(N(\text{H I})/\text{cm}^{-2})$	$20.60 \pm 0.10$
$[M/H]$	$-0.27 \pm 0.10$
$\Delta V_{90}$ ( $\text{km s}^{-1}$ )	$163 \pm 10$
$\log(N(\text{Zn II})/\text{cm}^{-2})$	$12.96 \pm 0.03$
$\log(N(\text{Mg I})/\text{cm}^{-2})$	$13.34 \pm 0.05$
$\log(N(\text{Cr II})/\text{cm}^{-2})$	$13.23 \pm 0.06$
$\log(N(\text{Ni II})/\text{cm}^{-2})$	$14.05 \pm 0.02$
$\log(N(\text{C I})/\text{cm}^{-2})$	$13.88^{+0.08}_{-0.04}$
$\log(N(\text{C I}^*)/\text{cm}^{-2})$	$14.0 \pm 0.2$
$\log(N(\text{C I}^{**})/\text{cm}^{-2})$	$< 13.5(2\sigma)$
H I 21 cm Optical depth	$< 0.13(3\sigma)$
Covering factor, $f$	0.93
Spin temperature (K)	$< 1895 \times (f/0.93)$

<sup>8</sup> <https://github.com/linetools/linetools>

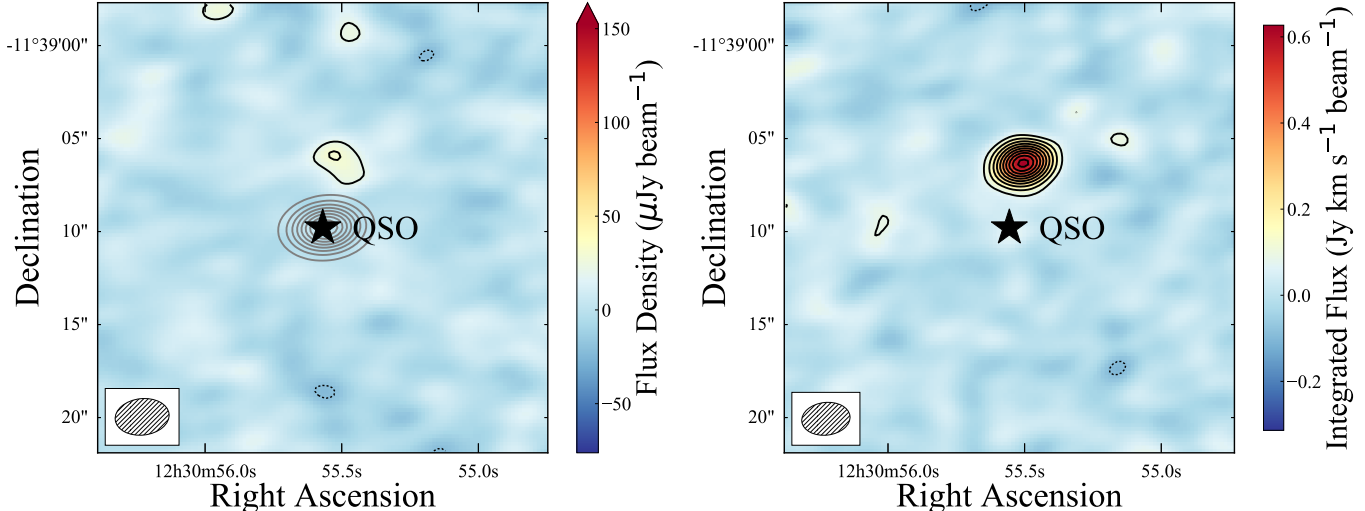


FIG. 2.— Left: 100.5 GHz continuum image of the field surrounding QSO B1228–113. To highlight the continuum emission of fainter sources, we have subtracted out the QSO emission (which was detected at very high signal-to-noise ratio). Gray contours start at  $300\sigma$  and increase by  $300\sigma$ , whereas black contours start at  $3\sigma$  and increase by  $\sqrt{2}\sigma$ . Right: Integrated CO(3–2) emission from the channels showing line emission (Figure 3). Contours begin at  $3\sigma$  and increase by  $2\sigma$ . Dotted contours indicate negative values. The synthesized beam is shown in the bottom left inset.

and Figure 3). The emission is spatially offset from the DLA by  $3.5''$  at a position angle of  $-14^\circ$ . Weak continuum emission is also detected at this location, with a flux density of  $46 \pm 10 \mu\text{Jy}$  (Figure 2). Both line and continuum emission from this source are spatially unresolved in the present ALMA images.

### 2.3. SINFONI Observations

The SINFONI spectrograph (Eisenhauer et al. 2003) on the VLT was used to obtain near-infrared integral field spectroscopy of the field surrounding QSO B1228–113 in program ID: 080.A-0742(A) (PI Peroux; see Péroux et al. 2011). We re-reduced the data using the ESO SINFONI pipeline v. 2.9. The final co-added data cube was scaled to match the previously measured flux of the integrated QSO spectrum (Ellison et al. 2005). This was necessary because the response functions of the flux calibrators for each night showed variations of  $\approx 50\%$ .

To measure possible  $\text{H}\alpha$  emission at the position of the ALMA CO(3–2) emission, we created a pseudo narrow-band image centered on the redshifted  $\text{H}\alpha$  line

at 2095.5 nm from the SINFONI data cube. Any potential continuum emission was subtracted from this image by interpolating the flux in adjacent wavelength intervals blueward and redward of the  $\text{H}\alpha$  line. The one dimensional spectrum (Figure 3: middle panel) was extracted with an aperture similar in size to the FWHM seeing of the observation. The spectrum shows an emission line that we identify as  $\text{H}\alpha$  at  $z = 2.1912$ . Besides  $\text{H}\alpha$ ,  $[\text{N II}] \lambda 6586$  is marginally detected as well. We fitted both emission lines with the Image Reduction and Analysis Facility package (IRAF; Tody 1993) using NGAUSSFIT and derived a total emission line flux of  $f(\text{H}\alpha) = (2.0 \pm 0.2) \times 10^{-17} \text{ erg s}^{-1} \text{ cm}^{-2}$  and  $f([\text{N II}]) = (0.5 \pm 0.3) \times 10^{-17} \text{ erg s}^{-1} \text{ cm}^{-2}$ , consistent with the previous flux limits (Péroux et al. 2011).

### 2.4. GMRT Observations

The 250 – 500 MHz receivers of the Giant Metrewave Radio Telescope (GMRT) were used to carry out a search for redshifted  $\text{H I}$  21 cm absorption from the DLA towards QSO B1228–113 on 2017 May 8. The GMRT Software Backend was used as the correlator with a bandwidth of 2.08 MHz centered at 444.85 MHz. The total velocity coverage is  $\approx 1400 \text{ km s}^{-1}$  at a velocity resolution of  $2.7 \text{ km s}^{-1}$ . The total on-source time was  $\sim 5$  hours, with 25 working antennas.

The GMRT data were analyzed in AIPS using standard procedures for low-frequency imaging and spectroscopy (e.g., Kanekar et al. 2014). The final spectral cube has an RMS noise of 1.7 mJy per  $2.7 \text{ km s}^{-1}$  channel, while the measured quasar continuum flux density is  $340.4 \pm 0.6 \text{ mJy}$ . The quasar spectrum shows no evidence for  $\text{H I}$  21 cm absorption, yielding a  $3\sigma$  upper limit on the velocity-integrated  $\text{H I}$  21 cm optical depth of  $0.13 \text{ km s}^{-1}$ , assuming a Gaussian line profile with a FWHM of  $20 \text{ km s}^{-1}$ . This implies a  $3\sigma$  lower limit of  $(2038 \times f) \text{ K}$  to the DLA spin temperature, where  $f$  is the DLA covering factor. Kanekar et al. (2009) used the Very Long Baseline Array (VLBA) to measure the

TABLE 2  
PROPERTIES OF THE GALAXY  
ALMA J123055.50–113906.4

Right Ascension (J2000)	12:30:55.50
Declination (J2000)	-11:39:06.4
Redshift of CO(3–2) emission	$2.1933 \pm 0.0005$
Redshift of $\text{H}\alpha$ /[N II] emission	$2.1912 \pm 0.0007$
$S_{\text{cont}}$ at $\nu_{\text{obs}} = 100.5 \text{ GHz}$ ( $\mu\text{Jy}$ )	$46 \pm 10$
FWHM <sub>CO(3–2)</sub> ( $\text{km s}^{-1}$ )	$600 \pm 60$
$\int S_{\text{CO(3–2)}} dv$ ( $\text{Jy km s}^{-1}$ )	$0.73 \pm 0.06$
$L_{\text{CO(3–2)}}$ ( $L_{\odot}$ )	$(2.5 \pm 0.2) \times 10^7$
$L'_{\text{CO(3–2)}}$ ( $\text{K km s}^{-1} \text{ pc}^2$ )	$(1.88 \pm 0.15) \times 10^{10}$
$f(\text{H}\alpha)$ ( $\text{erg s}^{-1} \text{ cm}^{-2}$ )	$(2.0 \pm 0.2) \times 10^{-17}$
$f([\text{N II}])$ ( $\text{erg s}^{-1} \text{ cm}^{-2}$ )	$(0.5 \pm 0.3) \times 10^{-17}$
$L_{\text{TIR}}$ ( $L_{\odot}$ )	$(2.2 \pm 0.5) \times 10^{12}$
$M_{\text{mol}}$ ( $M_{\odot}$ )	$(1.4 \pm 0.2) \times 10^{11}$
SFR <sub>H<math>\alpha</math></sub> ( $M_{\odot} \text{ yr}^{-1}$ )	$3.9 \pm 0.4$
SFR <sub>dust-corrected</sub> ( $M_{\odot} \text{ yr}^{-1}$ )	$110^{+60}_{-30}$

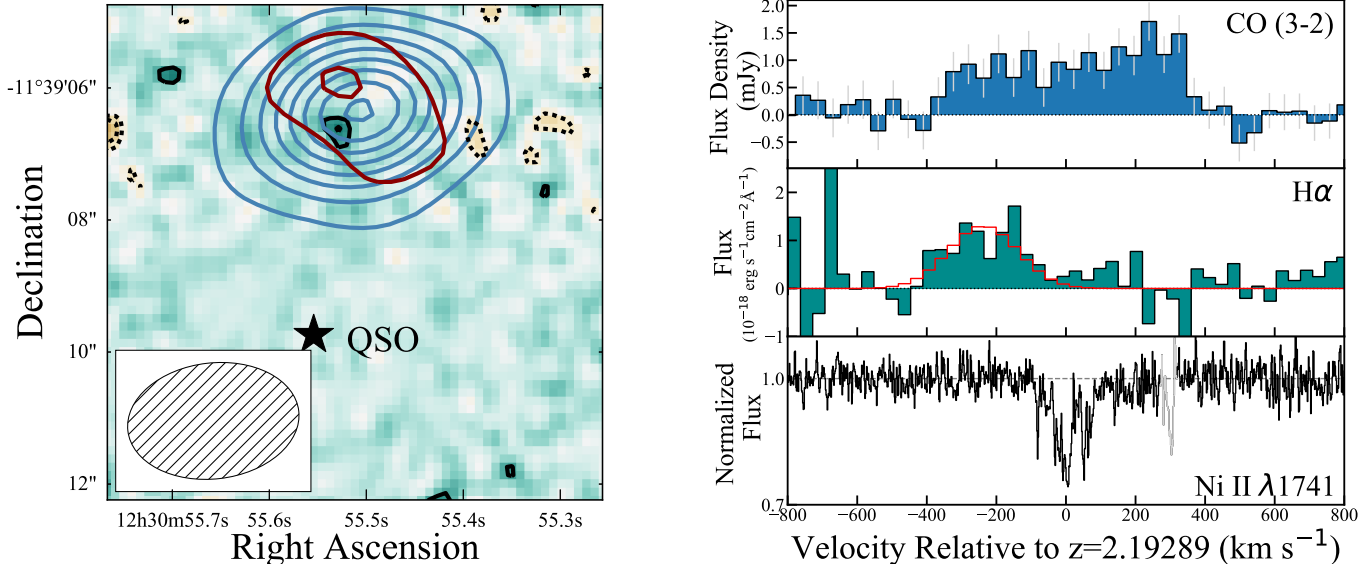


FIG. 3.— Left: H $\alpha$  (image and black contours), CO (blue contours) and 100.5 GHz continuum (dark red contours) emission. Outer contours are at  $3\sigma$ , with the contours increasing by  $\sqrt{2}\sigma$  for H $\alpha$  and the 100.5 GHz continuum, and by  $3\sigma$  for the CO(3–2) line. The emission peaks of all lines lies well within the ALMA synthesized beam (bottom left inset). Right: Spectra of the CO and H $\alpha$  emission lines, and a reference absorption line from the DLA (Ni II  $\lambda$ 1741); the CO emission and DLA absorption occur at a similar redshift, whereas the H $\alpha$  emission is slightly offset by  $\sim 220$  km s $^{-1}$ . This is similar to the absorber-galaxy pair discussed in Møller et al. (2018), who speculated this could be due to varying absorption across the galaxy. The Gaussian fit to the H $\alpha$  emission is shown in red.

core flux density of the quasar; combining the VLBA 327 MHz core flux density with the new GMRT total flux density yields a DLA covering factor of  $f = 0.93$ . The  $3\sigma$  lower limit to the DLA spin temperature is then  $T_s > 1895 \times (f/0.93)$  K.

### 3. RESULTS

#### 3.1. Galaxy Properties

We identify the line detected in the ALMA observations as the redshifted CO(3–2) emission line at  $z = 2.1933$ , in excellent agreement with the DLA absorption redshift,  $z = 2.19289$ . The velocity integrated CO(3–2) flux density of  $0.73 \pm 0.06$  Jy km s $^{-1}$  implies a CO(3–2) line luminosity of  $L'_{\text{CO}(3-2)} = (1.88 \pm 0.15) \times 10^{10}$  K km s $^{-1}$  pc $^2$  or  $L_{\text{CO}(3-2)} = (2.5 \pm 0.2) \times 10^7 L_{\odot}$ .

To estimate the total infrared luminosity [ $L(\text{TIR})$ ; defined as the integrated luminosity over the 8 – 1000  $\mu\text{m}$  wavelength range] from the ALMA 100.5 GHz continuum image, we fitted a modified black-body spectrum with mid-infrared slope,  $\alpha = 1.5$ , spectral emissivity index,  $\beta = 1.5$ , and dust temperature,  $T_{\text{dust}} = 35$  K, to the measured flux density (see e.g., Neeleman et al. 2017). This yields a total infrared luminosity of  $L(\text{TIR}) = (2.2 \pm 0.5) \times 10^{12} L_{\odot}$ . This estimate has a large systematic uncertainty ( $\sim 0.6$  dex) because both  $\beta$  and  $T_{\text{dust}}$  are not constrained by the single dust continuum measurement. We note, however, that this estimate is consistent with the estimate obtained from our  $L'(\text{CO})$  measurement, using the relationship between  $L'(\text{CO})$  and  $L(\text{TIR})$  in high- $z$  galaxies ( $L(\text{TIR}) = (2.2 \pm 1.5) \times 10^{12} L_{\odot}$ ; see e.g., Carilli & Walter 2013; Dessauges-Zavadsky et al. 2015).

From the H $\alpha$  detection, we estimate a dust-uncorrected star formation rate (SFR) of  $3.9 \pm 0.4 M_{\odot} \text{ yr}^{-1}$  (assuming a Kroupa initial mass function; Kennicutt & Evans 2012). Correcting this for dust obscuration using the to-

tal infrared luminosity (Kennicutt & Evans 2012) yields a dust-corrected SFR of  $110_{-30}^{+60} M_{\odot} \text{ yr}^{-1}$ , where the uncertainties include the systematic uncertainty on the total infrared luminosity. Comparison of the two SFRs suggest that the galaxy is highly dust-obscured, far more than typical galaxies at these redshifts (e.g., Moustakas et al. 2006). Only models with uncommonly low dust temperatures,  $T_{\text{dust}} \lesssim 25$  K, yield more typical dust-obscuration values, with dust-corrected SFRs  $\lesssim 20 M_{\odot} \text{ yr}^{-1}$ .

The molecular mass of the galaxy is estimated from the CO(3–2) line luminosity assuming a CO(3–2) to CO(1–0) line ratio of  $r_{31} = L'_{\text{CO}(3-2)}/L'_{\text{CO}(1-0)} = 0.57$  (Dessauges-Zavadsky et al. 2015) and a CO-to-H $_2$  conversion factor of  $\alpha_{\text{CO}} = 4.3 M_{\odot} (\text{K km s}^{-1} \text{ pc}^2)^{-1}$ . These assumptions are valid for typical star-forming galaxies (Bolatto et al. 2013), and yield a total molecular gas mass estimate of  $M_{\text{mol}} = (1.4 \pm 0.2) \times 10^{11} \times (\alpha_{\text{CO}}/4.3) \times (0.57/r_{31}) M_{\odot}$ . This is at the upper end of the molecular gas mass distribution for star-forming galaxies at this redshift (Tacconi et al. 2013; Genzel et al. 2015).

Note that if physical conditions are more akin to those in starburst galaxies, then  $\alpha_{\text{CO}} \approx 1 M_{\odot} (\text{K km s}^{-1} \text{ pc}^2)^{-1}$  and  $r_{31} \approx 1$ , yielding a molecular gas mass lower by a factor of  $\approx 10$ . However, we disfavor this scenario, as even the dust-corrected SFR estimate is significantly below the median SFRs seen in starburst galaxies (e.g. Daddi et al. 2005). We emphasize that, despite the uncertainty in  $\alpha_{\text{CO}}$  and  $r_{31}$ , this galaxy is likely massive, an assertion that is corroborated by the large CO(3–2) line width,  $\text{FWHM} \approx 600 \pm 60$  km s $^{-1}$  (Tiley et al. 2016).

#### 3.2. Galaxy/DLA Association

The agreement in redshift between the galaxy and DLA, as well as the low angular separation of the galaxy

from the quasar sightline ( $\approx 3.5''$  or  $\approx 30$  kpc at the DLA redshift), confirms the association between the molecular gas-rich galaxy and the high-metallicity absorber. This is consistent with results found at lower redshift, where CO emission studies of high-metallicity DLAs at  $z \approx 0.7$  (Møller et al. 2018; Kanekar et al. 2018) suggest that the cross-section for such DLAs appears to be biased toward galaxies with high molecular masses. Specifically, for 5 out of 7 targeted intermediate-redshift, high-metallicity absorbers, a galaxy with high molecular gas mass was found within  $\approx 50$  kpc of the DLA, and at the absorber redshift (Kanekar et al. 2018). Clearly a larger sample of CO observations surrounding high-metallicity  $z \sim 2$  DLAs is needed to confirm this assertion at these redshifts.

Of course there always is a possibility that the Ly- $\alpha$  absorption originates from a lower mass galaxy below the sensitivity threshold of the present ALMA observations. However, the VLT-SINFONI observations yield an upper limit to the SFR of such a putative galaxy of  $< 0.9 M_{\odot} \text{ yr}^{-1}$  (Péroux et al. 2011). In addition, we note that the excellent agreement in velocity between the centroid of the CO emission and the low-ionization metal line absorption ( $\approx 40 \text{ km s}^{-1}$ ; see Figure 3) disfavors scenarios where the absorber is probing gas with a bulk motion with respect to the galaxy — e.g., a single satellite galaxy or an extended disk — as in this case one would expect to see a net velocity offset between absorption and emission (Neeleman et al. 2016). The large velocity width of the DLA,  $\Delta V_{90} = 163 \pm 10 \text{ km s}^{-1}$  (see e.g., Prochaska & Wolfe 1997) is further evidence the DLA is associated with a more massive galaxy halo, (e.g., Ledoux et al. 2006) and large stellar mass ( $\log(M_*/M_{\odot}) \gtrsim 10.5$ ; Christensen et al. 2014).

### 3.3. Physical Conditions of the Absorbing Gas

The detection of C I in the UVES spectrum, indicates the presence of cold dense gas in the DLA, as C I has been linked to the presence of molecular hydrogen (e.g., Srianand et al. 2005). The C I absorption in the  $z = 2.19289$  DLA spans a wide range of velocities, indicating that the line-of-sight probes several distinct cold gas clumps. Interestingly, the strongest absorption component of the dominant low-ionization lines (e.g., Zn II) at  $v = 3 \text{ km s}^{-1}$  shows no C I absorption. This suggests that this component must be significantly warmer and less dense than the C I-bearing components.

This scenario is corroborated by our H I 21 cm absorption measurement. The high spin temperature, ( $T_s > 1895 \times (f/0.93) \text{ K}$ ), is inconsistent with the known anti-correlation between  $T_s$  and metallicity [M/H] (Kanekar et al. 2014). If, however, we assume that the H I is predominantly associated with the strongest Zn II absorption component, the metallicity of this gas is reduced to  $-0.7$ , which is consistent with the  $T_s$ -[M/H] anti-correlation. We note that this requires that approximately 50% of the metals are locked up in the denser phase traced by C I, and that this phase contribute little to the total H I column density.

This implies that either this phase is very metal-rich and small, thereby containing intrinsically little H I gas,

or that most of the H I has been converted into H<sub>2</sub>. However, a rough estimate of the H<sub>2</sub> column density from the expected scaling relations between C I and H<sub>2</sub> (Glover & Clark 2016) gives an H<sub>2</sub> column density of  $4 \times 10^{18} \text{ cm}^{-2}$ , well below the total H I content of the DLA but consistent with previous molecular hydrogen column density measurements in DLAs (e.g., Srianand et al. 2005). We therefore favor the first scenario whereby most of the metals are locked up in small metal-rich clumps. Similar multi-phase structure has been previously observed in a few high- $z$  absorbers (e.g., Noterdaeme et al. 2017; Rudie et al. 2017). Alternatively, the high inferred spin temperature might arise if the sightline towards the radio core has a significantly lower H I column density than that towards the optical QSO (e.g., Wolfe et al. 2003; Kanekar et al. 2014).

## 4. SUMMARY

We present, for the first time, molecular emission from a galaxy associated with a DLA at  $z \sim 2.2$ . Our results highlight the ability of ALMA to detect and characterize the galaxies associated with high-metallicity DLAs at the peak epoch of galaxy assembly. We obtain a high molecular gas mass,  $M_{\text{mol}} = (1.4 \pm 0.2) \times 10^{11} \times (\alpha_{\text{CO}}/4.3) \times (0.57/r_{31}) M_{\odot}$ , at the upper end of the mass distribution for star-forming galaxies at these redshifts (e.g., Tacconi et al. 2013; Genzel et al. 2015). The detection of far-infrared continuum with ALMA and weak H $\alpha$  emission indicates significant amounts of dust obscuration, and a dust-corrected SFR of  $\approx 110^{+60}_{-30} M_{\odot} \text{ yr}^{-1}$ .

The high molecular gas mass and large impact parameter ( $\approx 30$  kpc) are consistent with a scenario in which high-metallicity DLAs typically arise in the vicinity of massive gas-rich galaxies. Finally, the detection and non-detection, respectively, of C I and H I 21 cm absorption suggest that the H I along the sightline is predominantly warm, but that there are several cold dense gas components that contain  $\approx 50\%$  of the metals. The  $z = 2.19289$  DLA towards QSO B1228–113 thus highlights the power of combining absorption spectroscopy with emission line studies in order to study the multi-phase structure of the gas surrounding high redshift galaxies.

This paper makes use of ALMA data: ADS/JAO.ALMA#2016.1.00628.S. ALMA is a partnership of ESO (representing its member states), NSF (USA) and NINS (Japan), together with NRC (Canada) and NSC and ASIAA (Taiwan) and KASI (Republic of Korea), in cooperation with the Republic of Chile. The Joint ALMA Observatory is operated by ESO, AUI/NRAO and NAOJ. The National Radio Astronomy Observatory is a facility of the National Science Foundation operated under cooperative agreement by Associated Universities, Inc. MN acknowledges support from ERC Advanced Grant 740246 (Cosmic\_Gas). NK acknowledges support from the Department of Science and Technology via a Swarnajayanti Fellowship (DST/SJF/PSA-01/2012-13). LC acknowledges support from DFF-4090-00079. The Cosmic Dawn Center is funded by the DNRF.

## REFERENCES

- Akerman, C. J., Ellison, S. L., Pettini, M., & Steidel, C. C. 2005, *A&A*, 440, 499
- Bird, S., Vogelsberger, M., Haehnelt, M., et al. 2014, *MNRAS*, 445, 2313
- Bolatto, A. D., Wolfire, M., & Leroy, A. K. 2013, *ARA&A*, 51, 207
- Bouché, N., Murphy, M. T., Kacprzak, G. G., et al. 2013, *Science*, 341, 50
- Carilli, C. L., & Walter, F. 2013, *ARA&A*, 51, 105
- Chen, H.-W., Kennicutt, Jr., R. C., & Rauch, M. 2005, *ApJ*, 620, 703
- Christensen, L., Møller, P., Fynbo, J. P. U., & Zafar, T. 2014, *MNRAS*, 445, 225
- Daddi, E., Dickinson, M., Chary, R., et al. 2005, *ApJ*, 631, L13
- Dekker, H., D’Odorico, S., Kaufer, A., Delabre, B., & Kotzlowski, H. 2000, in *Proc. SPIE*, Vol. 4008, *Optical and IR Telescope Instrumentation and Detectors*, ed. M. Iye & A. F. Moorwood, 534–545
- Dessauges-Zavadsky, M., Zamojski, M., Schaerer, D., et al. 2015, *A&A*, 577, A50
- Eisenhauer, F., Abuter, R., Bickert, K., et al. 2003, in *Proc. SPIE*, Vol. 4841, *Instrument Design and Performance for Optical/Infrared Ground-based Telescopes*, ed. M. Iye & A. F. M. Moorwood, 1548–1561
- Ellison, S. L., Hall, P. B., & Lira, P. 2005, *AJ*, 130, 1345
- Ellison, S. L., Yan, L., Hook, I. M., et al. 2001, *A&A*, 379, 393
- Fumagalli, M., O’Meara, J. M., Prochaska, J. X., Rafelski, M., & Kanekar, N. 2015, *MNRAS*, 446, 3178
- Fumagalli, M., Mackenzie, R., Trayford, J., et al. 2017, *MNRAS*, 471, 3686
- Fynbo, J. P. U., Laursen, P., Ledoux, C., et al. 2010, *MNRAS*, 408, 2128
- Genzel, R., Tacconi, L. J., Lutz, D., et al. 2015, *ApJ*, 800, 20
- Glover, S. C. O., & Clark, P. C. 2016, *MNRAS*, 456, 3596
- Greisen, E. W. 2003, in *Astrophysics and Space Science Library*, Vol. 285, *Information Handling in Astronomy - Historical Vistas*, ed. A. Heck, 109
- Johnson-Groh, M., Marois, C., & Ellison, S. L. 2016, *ApJ*, 831, 49
- Jorgenson, R. A., & Wolfe, A. M. 2014, *ApJ*, 785, 16
- Jorgenson, R. A., Wolfe, A. M., & Prochaska, J. X. 2010, *ApJ*, 722, 460
- Kanekar, N., Lane, W. M., Momjian, E., Briggs, F. H., & Chengalur, J. N. 2009, *MNRAS*, 394, L61
- Kanekar, N., Prochaska, J. X., Smette, A., et al. 2014, *MNRAS*, 438, 2131
- Kanekar, N., Prochaska, J. X., Christensen, L., et al. 2018, *ApJ*, submitted
- Kennicutt, R. C., & Evans, N. J. 2012, *ARA&A*, 50, 531
- Krogager, J.-K., Møller, P., Fynbo, J. P. U., & Noterdaeme, P. 2017, *MNRAS*, 469, 2959
- Kulkarni, V. P., Woodgate, B. E., York, D. G., et al. 2006, *ApJ*, 636, 30
- Le Brun, V., Bergeron, J., Boisse, P., & Deharveng, J. M. 1997, *A&A*, 321, 733
- Ledoux, C., Petitjean, P., Fynbo, J. P. U., Møller, P., & Srianand, R. 2006, *A&A*, 457, 71
- McMullin, J. P., Waters, B., Schiebel, D., Young, W., & Golap, K. 2007, in *Astronomical Society of the Pacific Conference Series*, Vol. 376, *Astronomical Data Analysis Software and Systems XVI*, ed. R. A. Shaw, F. Hill, & D. J. Bell, 127
- Møller, P., Warren, S. J., Fall, S. M., Fynbo, J. U., & Jakobsen, P. 2002, *ApJ*, 574, 51
- Møller, P., Christensen, L., Zwaan, M. A., et al. 2018, *MNRAS*, 474, 4039
- Moustakas, J., Kennicutt, Jr., R. C., & Tremonti, C. A. 2006, *ApJ*, 642, 775
- Neeleman, M., Kanekar, N., Prochaska, J. X., et al. 2017, *Science*, 355, 1285
- Neeleman, M., Prochaska, J. X., Zwaan, M. A., et al. 2016, *ApJ*, 820, 39
- Noterdaeme, P., Krogager, J.-K., Balashev, S., et al. 2017, *A&A*, 597, A82
- Pérez-Ràfols, I., Font-Ribera, A., Miralda-Escudé, J., et al. 2018, *MNRAS*, 473, 3019
- Péroux, C., Bouché, N., Kulkarni, V. P., York, D. G., & Vladilo, G. 2011, *MNRAS*, 410, 2237
- Péroux, C., McMahon, R. G., Storrie-Lombardi, L. J., & Irwin, M. J. 2003, *MNRAS*, 346, 1103
- Prochaska, J. X., & Wolfe, A. M. 1997, *ApJ*, 487, 73
- Prochaska, J. X., Tejos, N., Crighton, N. H. M., et al. 2017, *linetools/linetools: Third Minor Release*, doi:10.5281/zenodo.1036773
- Rudie, G. C., Newman, A. B., & Murphy, M. T. 2017, *ApJ*, 843, 98
- Schmidt, M. 1959, *ApJ*, 129, 243
- Srianand, R., Petitjean, P., Ledoux, C., Ferland, G., & Shaw, G. 2005, *MNRAS*, 362, 549
- Tacconi, L. J., Neri, R., Genzel, R., et al. 2013, *ApJ*, 768, 74
- Tiley, A. L., Bureau, M., Saintonge, A., et al. 2016, *MNRAS*, 461, 3494
- Tody, D. 1993, in *Astronomical Society of the Pacific Conference Series*, Vol. 52, *Astronomical Data Analysis Software and Systems II*, ed. R. J. Hanisch, R. J. V. Brissenden, & J. Barnes, 173
- Wolfe, A. M., Gawiser, E., & Prochaska, J. X. 2005, *ARA&A*, 43, 861
- Wolfe, A. M., Prochaska, J. X., & Gawiser, E. 2003, *ApJ*, 593, 215